

The Shaped Pupil Coronagraph for Planet Finding Coronagraphy: Optimization, Sensitivity, and Laboratory Testing

N. Jeremy Kasdin^a, Robert J. Vanderbei^b,
Michael G. Littman^a, Michael Carr^c and David N. Spergel^c

^aMechanical and Aerospace Engineering, Princeton University, Princeton, NJ

^bOperations Research and Financial Engineering, Princeton University, Princeton, NJ

^cDept. of Astrophysical Sciences, Princeton University, Princeton, NJ

ABSTRACT

This paper summarizes our work designing optimal shaped pupils for high-contrast imaging. We show how any effective apodization can be created using shaped pupils and present a variety of both one-dimensional and azimuthally symmetric pupil shapes. Each pupil has its own performance advantage and we discuss the tradeoffs among various designs. Optimizations are typically performed by maximizing a measure of system throughput under constraints on contrast and inner working angle. We mention the question of sensitivity to aberrations. Controlling aberrations will be critical for any implementation of a planet-finding coronagraph. Finally, we present our first laboratory results testing a shaped pupil coronagraph.

1. INTRODUCTION

NASA's recent announcement that it plans to launch the Terrestrial Planet Finder-C by early next decade has intensified the study of coronagraph approaches. The current baseline design for TPF-C is for a 6×3.5 meter off-axis Cassegrainian optical telescope and a coronagraph to achieve the needed starlight rejection. We have been studying what we call shaped pupil coronagraphs as an alternative to the traditional Lyot coronagraph for the past four years.^{1, 2, 9-11} These are coronagraphs with apodized entrance pupils that rely solely on one/zero binary openings, resulting in a more manufacturable and robust design.

In this paper we review the optimization problem for high-contrast imaging and present a summary of all of our shaped pupil design families to date. We describe the various tradeoffs and the advantages each type brings to planet finding. We then briefly describe the various categories of errors for which the sensitivity of a shaped pupil coronagraph must be studied, highlighting progress and important issues. Finally, we present our first results measuring the psf of a shaped pupil coronagraph in the lab.

2. ELECTRIC FIELD AND PERFORMANCE METRICS

In all of the designs in this paper, we utilize only scalar far-field Fraunhofer diffraction theory. This reduces our optimization problems to analyzing the results of a family of Fourier (or Hankel) transforms. There are currently a number of groups studying the effects of full vector field propagation, some early results of which are in these proceedings; nevertheless, we restrict ourselves here to the Fraunhofer case. Thus, the image-plane electric field $E()$ produced by an on-axis plane wave and an apodized aperture defined by an *apodization function* $A()$ (note that shaped pupils are simply a special case of an apodized aperture where the apodization function is zero-one valued) is given by,

$$E(\xi, \zeta) = \int \int_S e^{-2\pi i(x\xi + y\zeta)} A(x, y) dx dy \quad (1)$$

Further author information: (Send correspondence to N.J.K.)
N.J.K.: E-mail: jkasdin@princeton.edu, Telephone: 1 609 258 5673

Likewise, for circularly symmetric pupils this can be written in polar coordinates and simplified to yield the Hankel transform,

$$E(\rho) = 2\pi \int_0^{1/2} J_0(2\pi r \rho) A(r) r dr \quad (2)$$

where J_0 denotes the zero-order Bessel function of the first kind.

Here we have normalized our coordinates so that the unitless pupil-plane “length” r is given as a multiple of the aperture D and the unitless image-plane “length” is given as a multiple of focal-length times wavelength over aperture ($f\lambda/D$) or, equivalently, as an angular measure on the sky, in which case it is a multiple of just λ/D . The rectangular coordinate version is similarly scaled.

For both square (rectangular) or circular apertures, the *point spread function (psf)* is the square of the electric field at the image plane. The planet finding optimization problem is to find the “best” apodization function, $A()$, that results in a psf with the needed contrast in the desired region of the image plane. The question of what defines the best function is critical in any optimization approach. In our work we employ three critical performance metrics. The first is *contrast*. We define contrast as the ratio of the image plane intensity at the planet location with the peak intensity of the psf, which in polar coordinates is given by,

$$E^2(\xi, \zeta)/E^2(0, 0).$$

We say that we have high-contrast when this ratio is very small. For planet finding, the consensus is that a contrast of 10^{-10} outside a predefined radius is necessary in order to image an Earth-like planet that is 1 AU from its Sun-like star.

The second metric is actually a pair, the *inner working angle (iwa)* and *outer working angle (owa)*, ρ_{iwa} and ρ_{owa} . We wish to design pupils that have high-contrast for all ρ 's in the interval $\rho_{iwa} \leq \rho \leq \rho_{owa}$.

The third metric is throughput, which is a surrogate for integration time. Integration time is critical for any planet finding telescope as smaller integration times relax requirements on system stability, simplify control, and increase the number of possible observations. Unfortunately, formulas for integration time depend upon the specific approach to analyzing the data for detection or characterization and can be quite complicated.¹ Instead, for the purposes of design, we use simpler measures of throughput. The most natural measure, and the one we use for all of our optimizations, is what we call the *Airy Throughput*, the amount of energy that falls into the main lobe of the PSF relative to the total energy conveyed through a fully open aperture. In polar coordinates this is given by,

$$\mathcal{T}_{Airy} = \frac{\int_0^{\rho_{iwa}} E^2(\rho) 2\pi \rho d\rho}{(\pi(1/2)^2)} = 8 \int_0^{\rho_{iwa}} E^2(\rho) \rho d\rho \quad (3)$$

A similar expression can be found for rectangular coordinates.² The optimization problem then becomes finding the apodization function that maximizes the throughput subject to constraints on contrast and inner and outer working angles.

3. SMOOTH APODIZATIONS

Before turning to shaped pupils, it is informative to study the problem of optimal smooth apodizations. This problem is not new; an excellent survey can be found in Jacquionot³ with more recent ideas in Indebetouw⁴ and Watson.⁵ Nisenson and Papoulios⁶ describe their concept of using an apodized square aperture for high-contrast, where discovery is made along the diagonals. The most important optimal apodization is due to Slepian,⁷ who introduced the prolate spheroidal wave function as the optimal 1-D telescope apodization. Slepian's one dimensional optimization problem asks for the function that concentrates as much light as possible into the central lobe of the finite Fourier transform. Slepian and Pollack⁸ derive a finite fourier transform analog of the uncertainty principal and show that the function that solves this optimization problem is the zero order prolate spheroidal wavefunction, that is, the solution to the wave equation in prolate spheroidal coordinates (there is also an elegant solution to this problem using the calculus of variations). Figure 1 shows this optimal apodization and Figure 2 shows the resulting one-dimensional psf. This psf has an inner working angle of $4 \lambda/D$ and an excellent Airy throughput of 25%.

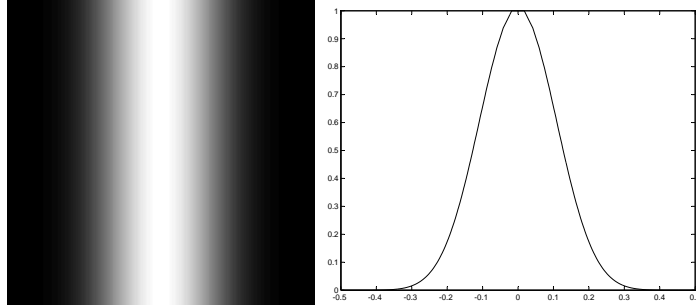


Figure 1. The optimal 1-D Slepian apodization function.

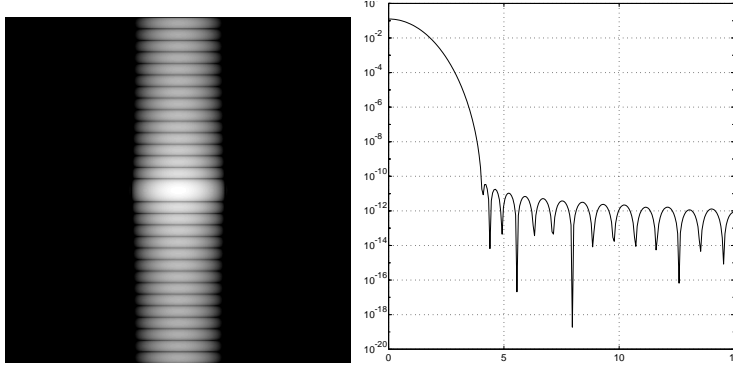


Figure 2. *Left* The PSF for the optimal 1-D Slepian smooth apodization in a square aperture. *Right* A cross section of the PSF showing the inner working angle of $4 \lambda/D$ and a contrast of 10^{-10} . This apodization has an Airy Throughput of 25%.

The one downside of the one-dimensional apodization is that it only achieves high contrast in two bands rather than a full 360 degrees around the star. Slepian⁷ also solved a similar optimization problem for the Hankel transform, finding the optimal circularly symmetric apodization, what he called the generalized prolate spheroidal wave function. Figure 3 shows this apodization along with its psf. Once again, the resulting psf has an inner working angle of $4 \lambda/D$ but now with a much wider discovery zone. However, this increase in the dark zone is obtained at the expense of throughput. The Airy throughput for this apodization is only 9%. We find that this tradeoff among contrast, inner working angle, throughput, and dark zone is a characteristic of the optimal high contrast problem. This throughput of 9% appears to be a fiducial value that all designs approach as we try to maximize the discovery zone.

4. OPTIMAL SHAPED PUPILS

While the smooth apodized pupils have some advantages, they are plagued by their extreme difficulty to manufacture. It is quite hard to produce a mask with the proper smoothly varying transmission in amplitude to the required accuracy. In addition, all smoothly varying masks also introduce complex phase shifts.² These problems, among others, led us to investigate the idea of shaped pupils. Rather than varying the throughput, we constrain the apodization function to be only zero-one valued. Our first mask was found by simply noting that a single shaped pupil in Eq. 1 reduces to a single, one-dimensional Fourier transform of the pupil contour. Thus, the optimal pupil is simply the prolate spheroidal wavefunction described earlier. Such a pupil is shown in Figure 4 along with its psf. As expected, this pupil has an iwa on the axis of $4 \lambda/D$ and a throughput of 43%. This high throughput, however, comes at the expense of the dark zone; this psf has a very narrow dark region and would require many rotations for complete discovery.

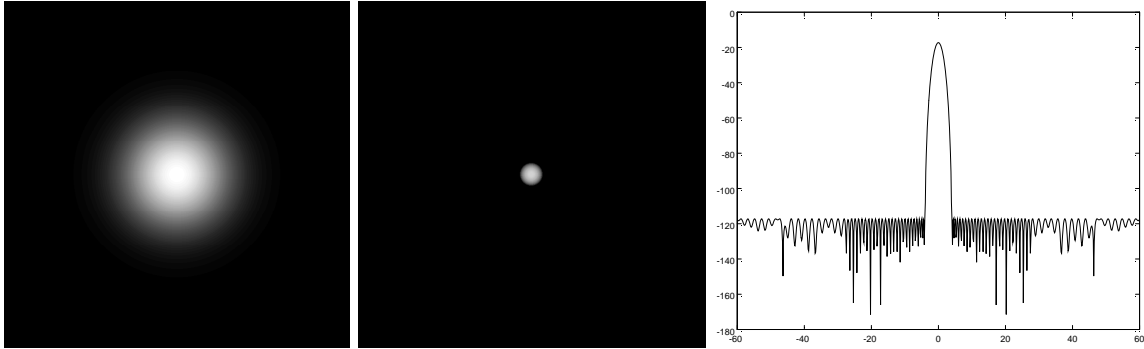


Figure 3. *Left* The optimal, smooth circularly symmetric apodization. *Center* The PSF for the optimal 2-D Slepian smooth apodization in a circular aperture. *Right* A cross section of the PSF showing the inner working angle of $4 \lambda/D$ and a contrast of 10^{-10} . This apodization has an Airy Throughput of 9%.

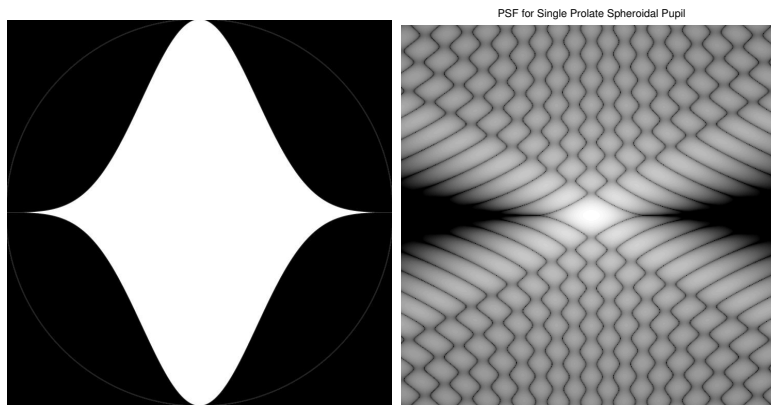


Figure 4. The single Spergel-Kasdin prolate-spheroidal mask and its point spread function. This mask has an iwa of $4 \lambda/D$ and a throughput of 43%.

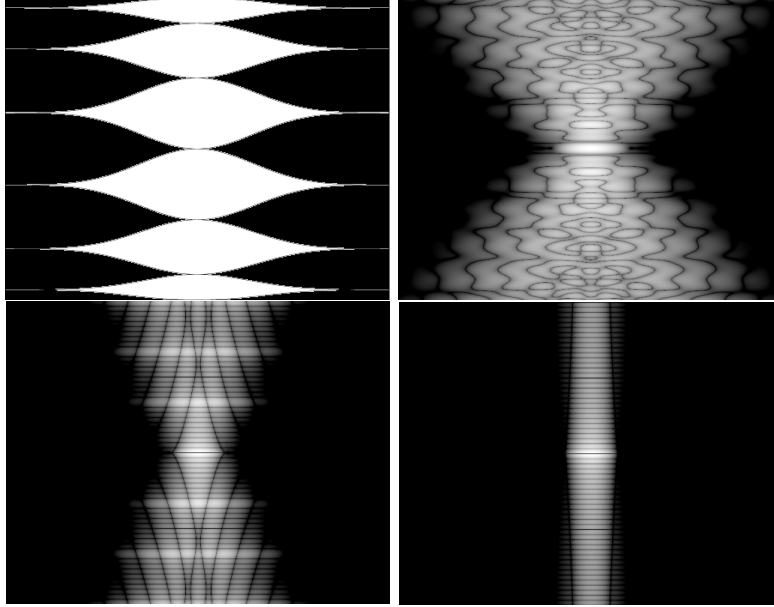


Figure 5. *Top Left* A six-pupil mask. *Top Right* Its corresponding image plane psf. *Bottom Left* The psf for a 10 pupil mask. *Bottom Right* The psf for a 100 pupil mask.

This discovery zone of this coronagraph can be increased by simply using more than one opening in the pupil. In fact, it can be shown that for a large number of repeated pupils, the psf approaches that of the 1-D smooth apodization.² Figure 5 shows a 6-pupil mask and its associated psf along with the psf's of a 10 pupil and 100 pupil mask. Of course, as the number of pupils increases, the throughput goes down and approaches the 25% of the smooth apodization. It is also worth noting that any one-dimensional apodization can be reproduced via the stacking of appropriate pupils.² The equivalent multi-pupil apodization for circularly symmetric masks is described in Vanderbei, et al..⁹

An alternative approach to multi-pupil design is to directly optimize the shape of each opening, again maximizing throughput under the constraint of high contrast.^{1,2} This provides more control over the shape of the discovery zone and thus potentially more throughput. Figure 6 shows a 6-opening pupil inscribed in an elliptical aperture. The iwa is $4 \lambda/D$ over a 45 degree arc and the Airy throughput is 30%. This pupil also has the added advantage that it can accommodate an 11% central obstruction. Because of the uniformity of the iwa, it only requires 4 rotations to cover the entire discovery space. It is also easier to make than previous multi-pupils, though the edge shapes can be quite complex.

The next family of shaped pupils arises from another optimization problem. If, rather than use Slepian's solution for the optimal apodizer, we instead formulate the apodization as a similar problem to find the function, we discover a new class of shaped pupils. By maximizing another measure of throughput (the pseudo-area, or the maximum value of the psf), subject to contrast constraints, we find that the optimal apodization is in fact zero-one valued.^{2,10} In polar coordinates this corresponds to a series of concentric rings of varying width. In a rectangular mask, this corresponds to a series of slots in the y -direction of varying width in the x -direction. We call this mask a *barcode mask*. Figure 7 shows an example of a concentric ring mask optimized for 10^{-10} contrast from 4 to $60 \lambda/D$. Its Airy throughput is back to 9%. Of course, this mask has the problem of not being manufacturable without laying it on glass, but it does have the advantage of covering the full discovery space. Vanderbei, et al..¹⁰ describe how spiders might be used to build such a mask.

Figure 8 shows a barcode mask optimized for the range of 4 to $40 \lambda/D$. It has an Airy throughput of 25%, but it would require at least one rotation. This mask has the advantage of being the easiest to build and to analyze.

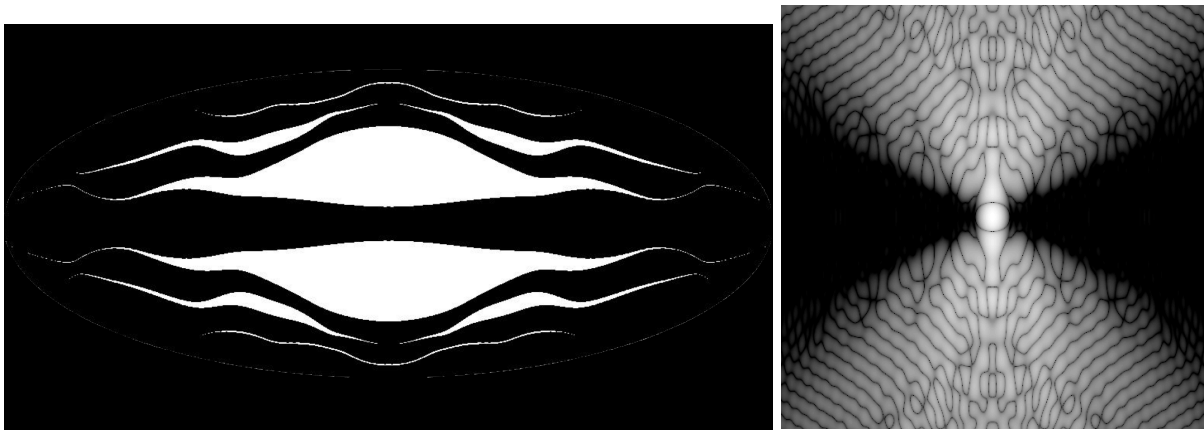


Figure 6. *Left* A six-pupil optimized mask inscribed in an elliptical aperture. *Right* Its corresponding image plane psf. This pupil has an iwa of $4 \lambda/D$ and an Airy throughput of 30%.

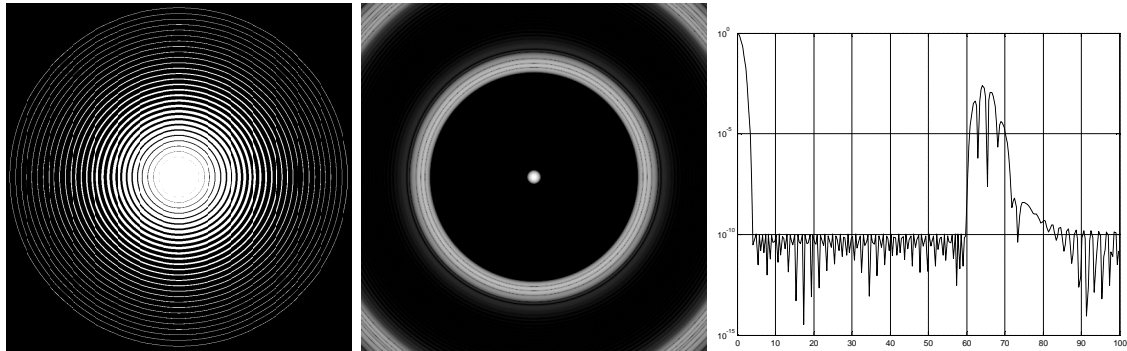


Figure 7. *Left* A concentric ring shaped pupil mask. *Center* The corresponding psf. *Right* A cross section of the psf. This pupil has an iwa of $4 \lambda/D$ and an Airy throughput of 9%.

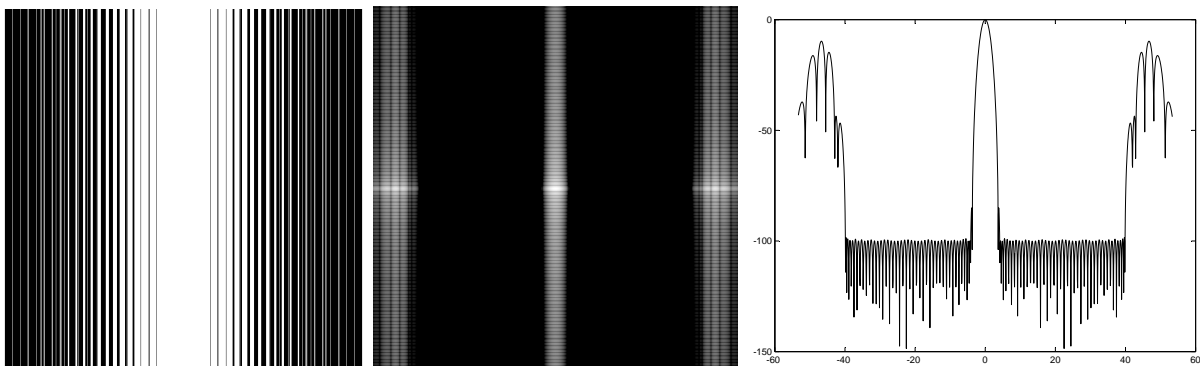


Figure 8. *Left* A barcode mask. *Center* The corresponding psf. *Right* A cross section of the psf. This pupil has an iwa of $4 \lambda/D$ and an Airy throughput of 25%.

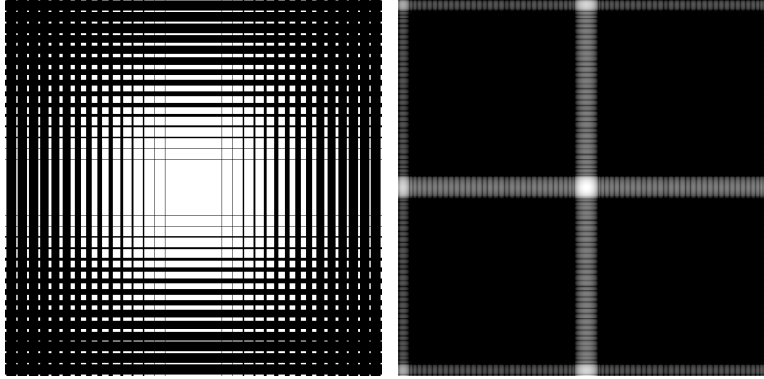


Figure 9. A checkerboard mask and its corresponding psf. This mask has an iwa of $2\sqrt{2} \lambda/D$ and an Airy throughput of 15%.

Our latest family of masks we call *checkerboard masks*. Here, we take advantage of the property in Eq. 1 that if $A(x, y)$ is a tensor product of two apodizations, $A(x)$ and $A(y)$, the electric field in the image plane is also a tensor product.¹¹ Thus, we design two barcode masks, each with a contrast of only 10^{-5} , and arrange them rotated 90 degrees. The resulting checkerboard mask has the desired contrast but at a much smaller inner working angle, though, as usual, with a throughput penalty. Figure 9 shows a checkerboard mask and its psf designed for an iwa (measured along the diagonal) of $2\sqrt{2}$ and an owa of $25 \lambda/D$. It has an Airy throughput of 15%. These masks also have the great advantage that each of the pair can easily be tested in the laboratory. In Vanderbei, et al.¹¹ we describe other variations on the checkerboard mask that can be used with a central obstruction or spiders or that use image plane masks to achieve even smaller inner working angles (though at large throughput penalties).

5. SENSITIVITY

A critical question for any shaped pupil coronagraph is its sensitivity to various types of errors. There are five error sources that are of most concern to the eventual performance of a shaped pupil system:

1. Mask accuracy.
2. Vector propagation and polarization.
3. Pointing error and nonzero stellar size.
4. Low-order aberrations.
5. Mid-spatial frequency phase and amplitude errors.

Item 5 is of great concern for all types of coronagraphs, as it produces speckle in the dark zone that can mask a planet. Little can be done in any coronagraph design to reduce sensitivity to these types of errors. Speckle must be reduced through the use of adaptive optics and a deformable mirror. Lowman, et al.¹² describes progress at JPL in high-contrast correction.

Item 4 refers to a reduction in contrast due to low-order aberrations in the telescope optics, such as defocus, tilt, coma, astigmatism, etc. It turns out that different types of coronagraphs can have dramatically different sensitivities to these errors. Green, et al.¹³ describes efforts at JPL and Princeton to compare the sensitivity of shaped pupil and Lyot coronagraphs to low order aberrations. These results indicate that a shaped pupil coronagraph can be up to 2 orders of magnitude less sensitive to certain aberrations than a Lyot coronagraph.

Traditional Lyot coronagraphs, as well as phase mask and nulling coronagraphs, are particularly sensitive to pointing error and finite stellar size. Small pointing errors can result in the star moving off the image plane



Figure 10. *Left* A four pupil mask made from Nickel via electroforming. *Right* An SEM image of the edge of the mask.

mask, producing a large light leak into the final image. In fact, Lyot coronagraphs demonstrate a θ^2 sensitivity to this type of error. In contrast, shaped pupil coronagraphs have no sensitivity to pointing error or finite stellar size—the psf simply moves on the image plane. There is some small sensitivity if a mask is used at a first image plane to prevent starlight from entering the camera, but this is quite relaxed.

Item 2 refers to the fact that all of the analyses and designs in this paper were performed using Fraunhofer diffraction theory. One would expect that a more careful examination of Maxell’s equations, including both polarizations and the interactions of the vector fields at the edges of the mask, would indicate some deviations from this simple scalar theory. There is concern that these deviations could produce unacceptable degradations in contrast. While we don’t believe this to be a significant problem due to the large size of the mask openings relative to the wavelength of light, it is an important question to be addressed. Lieber, et al.¹⁴ describes the early stages of our efforts to model and predict these effects.

Lastly, it is reasonable to ask how well these masks need to be made. Our studies and experiments show that the needed contrast can easily be achieved with current manufacturing capability. For example, in Kasdin, et al.² we describe an analysis to determine how well the slots need to be placed in a barcode mask. Assuming a random error in slot location, the standard deviation is given by,²

$$\sigma \leq \frac{10^{-5}|E_0(0,0)|}{\sqrt{2N}} \quad (4)$$

where N is the number of slots on half the mask. For the barcode mask shown in Fig. 8, which has 44 edges per side, this translates into a manufacturing accuracy on each edge of the mask of approximately 5×10^{-7} . For a 2 inch mask, this corresponds to a 25 nm accuracy requirement on the mask edges, something achievable with current fabrication technologies.

6. LABORATORY RESULTS

We have been developing a high-contrast coronagraph laboratory at Princeton to study the performance of various shaped pupil designs. This laboratory has recently been completed (February 2004) and we have just completed calibrations and alignments (May 2004). We report here our first results with shaped pupils. We are in the process of pursuing a variety of manufacturing technologies for producing shaped pupils, the most promising of which uses single-crystal silicon and a chemical etch. We currently have a single, high-quality shaped pupil produced using an electroforming process. It is shown in Fig. 10 along with a scanning electron microscope image of one of its edges. We have some concern that these rough edges will degrade performance but our capabilities have not been able to detect that yet.

Figure 11 shows the theoretical PSF for this pupil and the most recently measured PSF. Figure 12 shows a cross section of the PSF obtained from five exposures at different intensities. We are currently able to measure a contrast of up to $10^{-7.5}$ at an inner working angle of $5 \lambda/D$. Our biggest limitation is scattered light, primarily from the windows on the CCD camera, so we expect to do even better as we bring the scattered light under

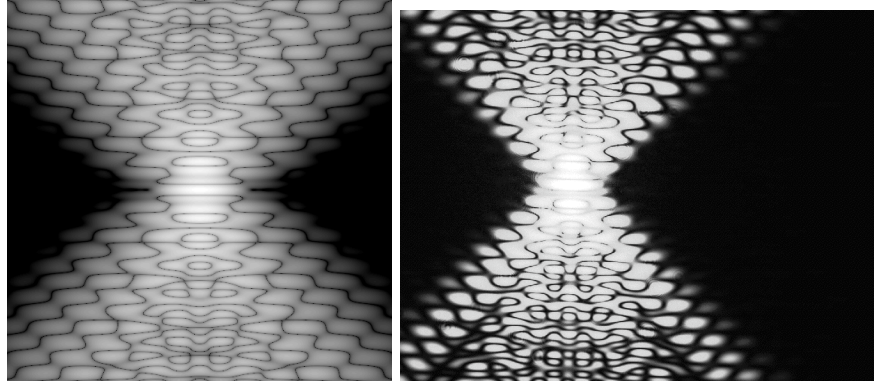


Figure 11. *Left* The theoretical PSF of the experimental mask. *Right* An experimental image of the four-pupil mask PSF.

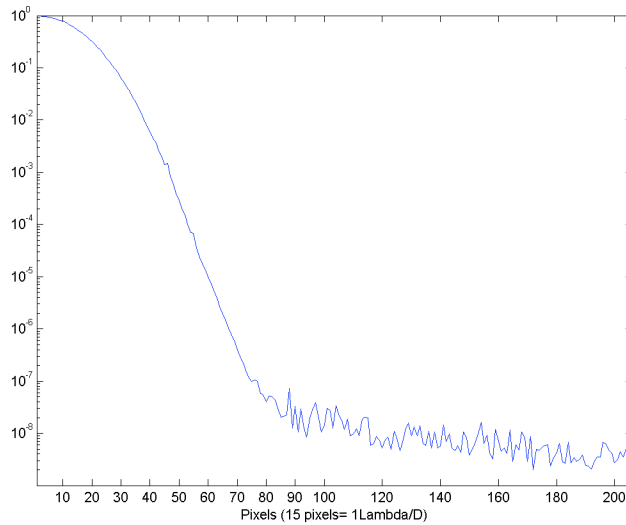


Figure 12. A cross section of the four-pupil PSF formed from 5 separate exposures of differing intensities. A contrast of $10^{-7.5}$ has been achieved at an iwa of $5 \lambda/D$. Contrast is currently limited by scattered light on the optical bench and the camera.

control. The scattered light in this image was reduced by tilting the camera relative to the incoming beam. All images were taken monochromatically using a He-Ne laser at 632.8 nm. The larger inner working angle is due to the rapid degradation of the four-pupil mask psf off the axis in the image plane. It is quite difficult to align the pupil with the camera pixels to reach the $4 \lambda/D$ designed for inner working angle. We are in the process of manufacturing masks with larger dark zones to eliminate this sensitivity.

7. FINAL REMARKS

In this paper we presented a summary overview of the various families of shaped pupil masks we have designed to date. All of these masks achieve high contrast by shaping the point spread function in the image plane in order to create a dark zone with a desired inner working angle. These masks can be used in square, circular, rectangular, or elliptical apertures, depending upon the needs of the mission. We argue on practical grounds that shaped-pupils are preferable to smooth apodizations; they are far easier and less expensive to manufacture.

While Lyot coronagraphs typically have more throughput than a shaped pupil coronagraph, they too suffer from manufacturing difficulties.

We also discussed the various sensitivity issues associated with coronagraph selection. We argue Lyot coronagraphs are also much more sensitive to pointing error and alignments as well as being more susceptible to low-order aberrations. Work is ongoing to study the more detailed response of shaped pupil coronagraphs with vector field theory. We also presented our first results measuring the psf of a shaped pupil coronagraph in the laboratory.

Final selection of a coronagraph for TPF is a number of years away, but we are rapidly developing a large family of options. The eventual choice will depend upon a complex tradeoff among inner working angle, throughput, discovery space, sensitivity, and robustness.

Acknowledgements

We gratefully acknowledge the support of the National Aeronautics and Space Administration through the Jet Propulsion Laboratory, California Institute of Technology for this work.

REFERENCES

1. N. J. Kasdin, R. J. Vanderbei, D. N. Spergel, and M. G. Littman, "Extrasolar planet finding via optimal apodized-pupil and shaped-pupil coronagraphs," *The Astrophysical Journal* **582**, pp. 1147–1161, January 2003.
2. N. J. Kasdin, R. J. Vanderbei, M. G. Littman, and D. N. Spergel, "Optimal asymmetric apodizations and shaped pupils for planet finding coronagraphy," *Applied Optics*, 2004. submitted.
3. P. Jacquinot and B. Roizen-Dossier, "Apodisation," *Progress in Optics* **3**, pp. 29–186, 1964.
4. G. Indebetouw, "Optimal apodizing properties of gaussian pupils," *Journal of Modern Optics* **37**(7), pp. 1271–1275, 1990.
5. S. M. Watson, J. P. Mills, S. L. Gaiser, and D. J. Diner, "Direct imaging of nonsolar planets with infrared telescopes using apodized coronagraphs," *Applied Optics* **30**(22), pp. 3253–3260, 1991.
6. P. Nisenson and C. Papaliolios, "Detection of earth-like planets using apodized telescopes," *The Astrophysical Journal* **548**(2), pp. L201–L205, 2001.
7. D. Slepian, "Analytic solution of two apodization problems," *Journal of the Optical Society of America* **55**(9), pp. 1110–1115, 1965.
8. D. Slepian and H. O. Pollack, "Prolate spheroidal wave functions, fourier analysis and uncertainty—i," *The Bell System Technical Journal*, pp. 43–84, January 1961.
9. R. Vanderbei, D. Spergel, and N. Kasdin, "Circularly symmetric apodization via starshaped masks," *Astrophysical Journal* **599**, pp. 686–694, December 10 2003.
10. R. Vanderbei, D. Spergel, and N. Kasdin, "Spiderweb masks for high contrast imaging," *Astrophysical Journal* **590**, pp. 593–603, June 10 2003.
11. R. J. Vanderbei, N. J. Kasdin, and D. N. Spergel, "Rectangular-mask coronagraphs for high-contrast imaging," *Astrophysical Journal* **615**, November 1 2004.
12. A. E. Lowman, J. T. Trauger, B. Gordon, J. J. Green, D. Moody, A. F. Niessner, F. Shi, and S. A. Macenka, "High-contrast imaging testbed for the terrestrial planet finder coronagraph," in *Proceedings of SPIE Conference on Astronomical Telescopes and Instrumentation*, 5487(178), 2004.
13. J. J. Green, S. B. Shaklan, R. J. Vanderbei, and N. J. Kasdin, "The sensitivity of shaped pupil coronagraphs to optical aberrations," in *Proceedings of SPIE Conference on Astronomical Telescopes and Instrumentation*, 5487(184), 2004.
14. M. D. Lieber, A. R. Neureuther, D. Ceperley, and N. J. Kasdin, "Vector wavefront propagation modeling for the tpf coronagraph," in *Proceedings of SPIE Conference on Astronomical Telescopes and Instrumentation*, 5487(180), 2004.